Electronic Supporting Information (ESI) for the manuscript:

Efficient Removal of Drugs of Abuse from Drinking Water by Metal-Organic Frameworks

Thais Grancha,[‡a] Patricia Garcia-Atienza,[‡b] Sergio Armenta,[b] José Manuel Herrero-Martínez,[*b] Rita Maria Percoco,[c] Donatella Armentano,[*c] Jesús Ferrando–Soria[a] and Emilio Pardo[*a]

[a]Instituto de Ciencia Molecular (ICMol), Universidad de Valencia, 46980 Paterna, Valencia, Spain. [b]Departamento de Química Analítica, Universitat de València, c/Dr. Moliner, 50, 46100 Burjassot, Valencia, Spain. [C]Dipartimento di Chimica e Tecnologie Chimiche (CTC), Università della Calabria, Rende 87036, Cosenza, Italy

Experimental Section

Materials. All chemicals were of reagent grade quality. They were purchased from commercial sources and used as received.

Preparation of MOFs and MTV-MOFs 1-6: $\{Ca^{II}Cu^{II}_6[(S,S)\text{-serimox}]_3(OH)_2(H_2O)\} \cdot 39H_2O$[1,2] (**1**), $\{Sr^{II}Cu^{II}_6[(S,S)\text{-Mecysmox}]_3(OH)_2(H_2O)\}\cdot 15H_2O$[3,4] (**2**), $\{Ca^{II}Cu^{II}_6[(S,S)\text{-methox}]_3(OH)_2(H_2O)\} \cdot 16H_2O$[5,6] (**3**), $\{Ca^{II}Cu^{II}_6[(S,S)\text{-methox}]_{1.5}[(S,S)\text{-serimox}]_{1.50}(OH)_2(H_2O)\} \cdot 30H_2O$[7] (**4**), $\{Sr^{II}Cu^{II}_6[(S,S)\text{-methox}]_{1.5}[(S,S)\text{-Mecysmox}]_{1.50}(OH)_2(H_2O)\} \cdot 36H_2O$[8,9] (**5**) and $\{Ca^{II}Cu^{II}_6[(S,S)\text{-serimox}]_2[(S,S)\text{-hismox}]_1\ (OH)_2(H_2O)\} \cdot 27H_2O$[10] (**6**) [where serimox = bis[(*S*)-serine]oxalyl diamide; Mecysmox = bis[*S*-methylcysteine]oxalyl diamide, methox = bis[(*S*)-methionine]oxalyl diamide and hismox = bis[(*S*)-histidine]oxalyl diamide] have been prepared, as polycrystalline powders, as previously reported. On the other side, aiming at crystallographic determination of host-guest adsorbates, well-shaped hexagonal prisms of **2** and **3**, suitable for SCXRD, were obtained by slow diffusion methods as reported previously. [6,10]

Preparation of $C_9H_{13}N@\{Sr^{II}Cu^{II}_6[(S,S)\text{-Mecysmox}]_3(OH)_2(H_2O)\} \cdot 6H_2O$ (amphetamine@2'), $C_9H_{13}N@\{Ca^{II}Cu^{II}_6[(S,S)\text{-methox}]_3(OH)_2(H_2O)\} \cdot 4H_2O$ (amphetamine@3) and $C_9H_{10}NO@\{Sr^{II}Cu^{II}_6[(S,S)\text{-methox}]_3(OH)_2(H_2O)\} \cdot 5H_2O$ (fentanyl'@3'): Well-shaped hexagonal prisms of **amphetamine@2'**, **amphetamine@3** and **fentanyl'@3'** suitable for SCXRD, could be obtained by soaking crystals of the corresponding MOF (**2'**, **3** or **3'**) (*ca.* 5.0 mg) for a week in saturated acetonitrile solutions containing amphetamine or fentanyl (recharging fresh saturated solutions daily). After this period, they were isolated by filtration, air-dried and characterized by SCXRD, PXRD (Figures S13-S15), C, H, N, S and TGA analyses (Figure S17) to obtain their chemical formulas. Anal.: calcd. for **amphetamine@2'**:

$C_{39}Cu_6SrS_6H_{65}N_7O_{27}$ (1725.3): C, 27.15; H, 3.80; S, 11.15; N, 5.68% Found: C, 27.09; H, 3.67; S, 11.12; N, 5.68%; IR (KBr): ν = 1608 and 1602 cm^{-1} (C=O). Anal.: calcd. for **amphetamine@3**: $C_{45}Cu_6CaS_6H_{73}N_7O_{25}$ (1725.8): C, 31.32; H, 4.26; S, 11.15; N, 5.68% Found: C, 31.39; H, 4.02; S, 11.17; N, 5.68%; IR (KBr): ν = 1611 and 1604 cm^{-1} (C=O). Anal.: calcd. for **fentanyl'@3'**: $C_{45}Cu_6SrS_6H_{72}N_7O_{27}$ (1804.4): C, 29.95; H, 4.02; S, 10.66; N, 5.43% Found: C, 30.09; H, 3.99; S, 10.57; N, 5.38%; IR (KBr): ν = 1605 cm^{-1} (C=O).

Physical Techniques: Elemental (C, H, S, N) and ICP analyses were performed at the Microanalytical Service of the Universitat de València. FT–IR spectra were recorded on a Perkin-Elmer 882 spectrophotometer as KBr pellets. The thermogravimetric analyses were performed on crystalline samples under a dry N_2 atmosphere with a Mettler Toledo TGA/STDA 851^e thermobalance operating at a heating rate of 10 ºC min^{-1}.

The N_2 adsorption-desorption isotherms at 77 K were carried out on crystalline samples of **amphetamine@2'**, **amphetamine@3** and **fentanyl@3'** with a Belsorp MINI X instrument. Samples were activated at 70 °C under reduced pressure (10^{-6} Torr) for 16 h prior to carry out the sorption measurements.

Analytical experiments:

- Capture experiments:

To conduct capture studies, an SPE protocol was implemented, which can be summarized as follows. SPE cartridges were prepared as previously described. Aqueous standard mixtures (1 mL) containing target drugs were loaded onto the SPE cartridge, followed by a 2 mL water washing. Elution was performed with 5 mL of methanol (MeOH), and the cartridge was reconditioned with 1 mL each of MeOH and water. All SPE fractions were filtered through a 0.22 µm membrane and injected into the HPLC-

MS system. The integrity of the MOFs after each capture experiment was repeatedly verified through ICP-MS analysis, which confirmed that no metal leaching occurred in any of the experiments. Please note, the studies shown in this manuscript that involve the use of illegal drugs have been performed ethically and in accordance with legislation (see Notes). The present study has been performed in deionized water, as the illegal nature of the studied contaminants have precluded to have most of them widely available to perform studies using real samples, as it has been performed in other studies developed by some of us.[9,11,12]

- Reusability experiments:

To perform reusability studies, the same SPE protocol as for capture experiments was implemented but using 1 mL of 20 μg L^{-1} fentanyl aqueous solution and analyze the eluents after each cycle. The powdered activated carbon (PAC) used for comparison was purchased from Sigma-Aldrich (CAS: 7440-44-0) and used as received.

- Reagents and materials:

Standard solutions of fentanyl, nicotine, lysergic acid diethylamide (LSD), ketamine, amphetamine, methamphetamine, benzoylecgonine, cocaine, 3-Methoxyphencyclidine (3-MeO-PCP), butylone, cathinone, methylone, heroin, 3,4-methylenedioxymethamphetamine (MDMA), alpha-pyrrolidinovalerophenone (α-PVP), caffeine, diazepam, codeine, oxazepam, norketamine, ecgonine methyl ester (EME), 6-monoacetylmorphine (6-MAM), alprazolam, methadone, buprenorphine, tramadol, chlordiazepoxide, naphazoline, and clorazepate, and the corresponding deuterated internal standards were obtained from Sigma (Stenheim, Germany). See details and structures in Schemes S1-S3. All the solvents (*e.g.* methanol (MeOH) or acetonitrile (MeCN) and others) were all HPLC grade and purchased from VWR International Eurolab (Barcelona, Spain). Nanopure water was purified in Crystal B30 EDI Adrona

deionizer (Riga, Latvia). Other non-specific reagents were of analytical grade unless otherwise stated. SPE propylene cartridges of 1mL (internal volume) and their respective frits (1/16′, 20 μm) were provided from Análisis Vínicos (Tomelloso, Spain). A multicomponent stock solution was prepared at 10 mg L^{-1} concentration level in MeOH and stored at -20 °C in amber glass vial. Standard mixtures were prepared by dilution of this stock solution. Calibration curves ranging from 1 to 100 μg L^{-1} were also prepared by diluting this multicomponent stock solution in water. The powdered activated carbon (PAC) used for reusability experiments was purchased from Sigma-Aldrich (CAS: 7440-44-0) and used as received.

- Instrumentation:

For the solid-phase extraction (SPE) protocols, manifold (VacElut) with twelve positions (Agilent Technologies, Waldbronn, Germany,) and pump for vacuum N938 Laboport (KNF, Freiburg, Germany) were used. For HPLC-tandem mass spectrometry (MS/MS) analysis, an AB SCIEX (Redwood City, CA, USA) ExionLC AD coupled to a Sciex QTRAP 6500+ mass spectrometer system was employed. Separations were performed in a C18 Kinetex chromatographic column (100 × 2.1 mm, 1.7 μm particle size) from Phenomenex (Torrance, CA, USA), and a 0.4 mL min^{-1} mobile phase flow rate. The mobile phase was made up of 0.2% formic acid (v/v) and 2 mM ammonium formate in water (A) and MeCN (B), using a gradient from 5 to 30% B for 6 min, from 30 to 50% B for 2 min, and from 50 to 100% B for 4 min. MS/MS acquisitions were done using electrospray ionization, with a source temperature of 550 °C and an ion spray voltage of 5.5 kV. Data were evaluated using the PeakView™ software from AB SCIEX. To perform quantitation of analytes, multiple reaction monitoring (MRM) mode was used. Two MRM transitions were obtained for each drug separately by direct infusion of a concentrated standard (see Table S3).

X-ray crystallographic data collection and structure refinement: Crystals of **amphetamine@2'**, **amphetamine@3** and **fentanyl'@3'** were selected and mounted on a MITIGEN holder in Paratone oil. Due to the stability of all the three samples at air, they were measured at room temperature in order to extract the best data set avoiding the possible amorphous contribution of disordered solvent lattice molecules. Diffraction data for **amphetamine@2'**, **amphetamine@3** and **fentanyl'@3'** were acquired on a Bruker-Nonius X8APEXII CCD area detector diffractometer using graphite-monochromated Mo-Kα radiation (λ = 0.71073 Å), as a significant beam-damage was observed for both single crystals under synchrotron radiation. Bearing in mind that crystal structure of adsorbates **amphetamine@2'**, **amphetamine@3** and **fentanyl'@3'** have been obtained measuring on crystals that suffered a single-crystal to single-crystal (SC to SC) process, it is reasonable. The data were processed through SAINT[13] reduction and SADABS[14] multi-scan absorption software. The structures were solved with the SHELXS structure solution program, using the Patterson method. The model was refined with version 2019/1 of SHELXL against F^2 on all data by full-matrix least squares.[15–17]

We could measure on **fentanyl'@3** at synchrotron, after loading guests, in order to go deep in the point of statistical disorder we observe for the guest molecules. However, despite the good data quality of data set measured, appreciable crystal decay has been detected and no noticeable variations in the final best model of crystal structure have been achieved for **fentanyl'@3**.

In all samples, all non-hydrogen atoms of the networks were refined anisotropically, except highly dynamically disordered atoms of guest molecules refined with restraints and constraints of rigid groups. For such kind of single crystals, the lower data quality for adsorbates, embedding highly disordered guest molecules, makes the use of

constraints and especially restraints essential. The use of some bond lengths restraints applied on atoms belonging to highly dynamic moieties, has been reasonably imposed and related to the expected thermal motion, likely depending on the large pore's size of the frameworks (FLAT, DFIX, DANG, SIMU, DELU and ISOR). Aminoacidic chains in all the three samples have been systematically refined with restrains on C-C and C-S bond lengths, and in **amphetamine@2'** one of the two crystallographically not equivalent methylcysteine chains was totally fixed (with AFIX 1) in the final refinement to reach convergence. In their refinements some further restraints, to make the refinement more efficient, have been applied. For instance, ADP components have been restrained to be like other related atoms, using SIMU 0.04 for disordered sections or EADP for group of atoms of the guest molecules expected to have essentially similar ADPs. In the network of the **amphetamine@3** MOF, all the hydrogen atoms of the networks were set in calculated position and refined isotropically using the riding model and hydrogen atoms on the guest molecules and on the solvent lattice molecules were neither found nor calculated. In fact, it is often expected that guest molecules are severely disordered, as a direct consequence of their high thermal motion and exhibited statistic disorder.

On the contrary, in **amphetamine@2'**and **fentanyl'@3**, due to the impressive statistical disorder, other than dynamical one, hydrogen atoms where not defined neither for network nor for the guest molecules.

It should be also underlined that our best model has taken into account the most persistence conformations –within the additional complication– that even a low percentage, not taken into account, such as a 10% of a whole drugs guest molecule, is still a significant amount of electron density, and whole-molecule disorder lurks everywhere in the inky shadows of structure refinement, affecting quality of the model.

In all adsorbate's crystal structure refinements, the occupancies of the guests in the pores were fixed at 0.333, in good agreement with bulk CHN analysis. Unfortunately, also thermal motion has not been refined for disordered sites, for which after a first four cycles of refinements it was blocked. We strongly believe that it is the more reliable way to attempt to define loading instead of taking into account merely thermal factors, which can be affected by a lot of issues above all severe disorder.

As stated above and as expected, in all adsorbates guest molecules are statistically and thermally disordered. In **fentanyl'@3',** fentanyl' fragments are severely disordered exhibiting three set of possible orientations of the guest molecules as detailed in Figure S11. This imposed the use of further constrains to block atoms of the fentanyl fragment representing terminal groups during the final refinement. The partial overlap between different orientations at atom sites, together with thermal disorder of thioether chains of the methionine residues makes the final refinement really challenging (Figure S11) without reaching a suitable level of convergence. It is a poorly behaved structure, here parameters related to disordered fragments remain constantly oscillating even if appropriate restraints have been introduced to stabilise oscillating parameters.

Finally, the estimated empty volumes for **amphetamine@2'**, **amphetamine@3** and **fentanyl'@3'** without the crystallization water molecules is 550.6(1), 227.5 (2) and 137.3 (3) $Å^3$, values which represent *ca.* 15.0, 6.4 and 3.8 %, respectively, of potential void per unit cell volume [V = 3667.8(1), 3567.0 (2) and 3630.1(3) $Å^3$]. In accordance with BET and SCXRD analysis (Figures S1 and S13-S15), the channels of **2**, **3** and **3'** are entirely filled by drug molecules (and solvent molecules in **2'**).

A summary of the crystallographic data and structure refinement for the three compounds is given in Table S2. The comments for the alerts A and B are reported in the CIFs using the validation response form (vrf). CCDC reference numbers are

2415524 – 2415526 for **amphetamine@2'**, **amphetamine@3** and **fentanyl'@3'**, respectively.

The final geometrical calculations on free voids and the graphical manipulations were carried out with PLATON[18,19] implemented in WinGX,[20] and CRYSTAL MAKER[21] programs, respectively.

X-ray Powder Diffraction Measurements: Fresh polycrystalline samples of **2'**, **3**, **3'**, **amphetamine@2'**, **amphetamine@3** and **fentanyl'@3'** were introduced into 0.5 mm borosilicate capillaries prior to being mounted and aligned on an Empyrean PANalytical powder diffractometer, using Cu Kα radiation (λ = 1.54056 Å). For each sample, five repeated measurements were collected at room temperature (2θ = 2–60°) and merged in a single diffractogram.

Microscopy measurements. Scanning Electron Microscopy (SEM) images and elemental analysis was carried out for MOF **3**, using a HITACHI S−4100 electron microscope coupled with an Energy Dispersive X–ray (EDX) detector. Data was analysed with EMIP 3.0. Transmission Electron Microscopy (SEM) images were obtained with a JEOL jem 1010 high contrast transmission electron microscope equipped with an 8 Mpx AMT digital camera.

Table S1. Summary of Crystallographic Data for **amphetamine@2', amphetamine@3 and fentanyl'@3'**

Compound	**amphetamine@2'**	**amphetamine@3**	**fentanyl'@3'**
Formula	$C_{39}H_{65}SrCu_6N_7O_{27}S_6$	$C_{45}H_{73}CaCu_6N_7O_{25}S_6$	$C_{45}H_{72}SrCu_6N_7O_{27}S_6$
M (g mol^{-1})	1725.20	1725.78	1804.31
λ (Å)	0.71073	0.71073	0.71073
Crystal system	hexagonal	hexagonal	hexagonal
Space group	$P6_3$	$P6_3$	$P6_3$
a (Å)	18.1039(12)	17.574(4)	17.9618
c (Å)	12.9220(9)	13.335(5)	12.9922(12
V (Å^3)	3667.79(2)	3567(2)	3630.1 (6)
Z	2	2	2
ρ_{calc} (g cm^{-3})	1.562	1.607	1.651
μ (mm^{-1})	2.671	2.079	2.702
T (K)	296	296	296
θ range for data collection (°)	2.250 to 26.464	1.338 to 26.534	2.042 to 26.317
Completeness to θ = 25.0	100%	100%	100%
Measured reflections	85766	49547	84175
Unique reflections (Rint)	5015 (0.1738)	4892 (0.0563)	4934 (0.1001)
Observed reflections [$I > 2\sigma(I)$]	3002	3690	3515
Goof	1.000	1.598	1.552
Absolute structure parameter (Flack)	0.37(2)	0.19(2)	0.37(2)
R^a [$I > 2\sigma(I)$] (all data)	0.0819 (0.1459)	0.0709 (0.0970)	0.0745 (0.1075)
wR^b [$I > 2\sigma(I)$] (all data)	0.2306 (0.2774)	0.2146 (0.2293)	0.2176 (0.2355)
CCDC	2415524	2415525	2415526

^{a} $R = \sum(|F_o| - |F_c|)/\sum|F_o|$. ^{b} $wR = [\sum w(|F_o| - |F_c|)^2/\sum w|F_o|^2]^{1/2}$.

Table S2. Removal efficiency (%) of fentanyl, for 16 consecutive cycles, using 10 mg L^{-1} aqueous samples.

Reuses	MOF-3	GAC
1	99±2	100±2
2	99±3	99±2
3	100±2	99.7±1.7
4	100±3	99±2
5	99.5±1.0	99.3±1.6
6	100±2	100±3
7	99±2	99.5±1.2
8	99±3	99±3
9	99.3±1.3	98±3
10	99.2±1.5	99.0±1.6
11	99±3	98±3
12	99±2	98±2
13	99±3	97±2
14	99±3	96.5±1.1
15	99±2	96±2
16	99±3	95±2

Table S3. Summary of MRM transitions for the determination of the different drugs under study.

Analyte	t_R (min)	Q1 (m/z)	Q3 quantifier (m/z)	Q3 qualifier (m/z)	Internal standard
Fentanyl	9.29	337	188	105	Fentanyl-D5
Fentanyl-D5	9.29	342	188	-	-
Nicotine	1.40	163	130	132	Nicotine-D4
Nicotine-D4	1.40	167	136	-	-
LSD	8.80	324	223	208	LSD-D3
LSD-D3	8.80	327	226	-	-
Ketamine	7.62	238	125	180	Ketamine-D4
Ketamine-D4	7.62	242	129	-	-
Amphetamine	5.78	136	119	91	Amphetamine-D5
Amphetamine-D5	5.78	141	93	-	-
Methamphetamine	6.15	150	91	-	Methamphetamine-D5
Methamphetamine-D5	6.15	155	91	-	-
Benzoylecgonine	8.00	290	77	105	Benzoylecgonine-D3
Benzoylecgonine-D3	8.00	293	105	-	-
Cocaine	8.44	304	182	105	Cocaine-D3
Cocaine-D3	8.44	307	185	-	-
3-MeO-PCP	9.29	274	189	121	MDMA-D5
Butylone	6.84	222	131	191	Butylone-D3
Butylone-D3	6.84	225	177	-	-
Cathinone	4.60	150	132	117	Cathinone-D5
Cathinone-D5	4.60	155	137	-	-
Methylone	5.87	208	160	132	MDMA-D5
Heroine	8.38	370	268	165	Heroine-D9
Heroine-D9	8.38	379	272	-	-
MDMA	6.48	194	163	105	MDMA-D5
MDMA-D5	6.48	199	165	-	-
α-PVP	8.24	232	91	126	MDMA-D5
Caffeine	7.16	195	138	110	MDMA-D5
Diazepam	11.01	285	154	193	Oxazepam-D5
Codeine	5.96	300	115	152	Ketamine-D4
Oxazepam	10.37	287	241	269	Oxazepam-D5
Oxazepam-D5	10.37	292	246	-	-
Norketamine	7.42	224	207	125	Norketamine-D4
Norketamine-D4	7.42	228	211	-	-
EME	0.73	200	182	82	Cocaine-D3
6-MAM	6.57	328	165	211	MDMA-D5
Alprazolam	10.52	309	281	205	Aprazolam-D5
Alprazolam-D5	10.52	314	386	-	-
Methadone	9.99	310	265	105	Methadone-D5
Methadone-D5	9.99	313	268	-	-
Buprenorphine	9.58	468	55	414	MDMA-D5
Tramadol	8.12	264	58	42	MDMA-D5

Chlordiazepoxide	8.85	300	283	227	MDMA-D5
Naphazoline	7.83	211	141	115	MDMA-D5
Clorazepate	10.55	271	140	165	MDMA-D5

[a]LSD = Lysergic acid diethylamide, [b] 3-MeO-PCP = 3-Methoxyphencyclidine, [c]MDMA = 3,4-methylenedioxymethamphetamine [d]α-PVP = alpha-Pyrrolidinovalerophenone, [e]EME = Ecgonine methyl ester. [f]6-MAM = 6-Monoacetylmorphine.

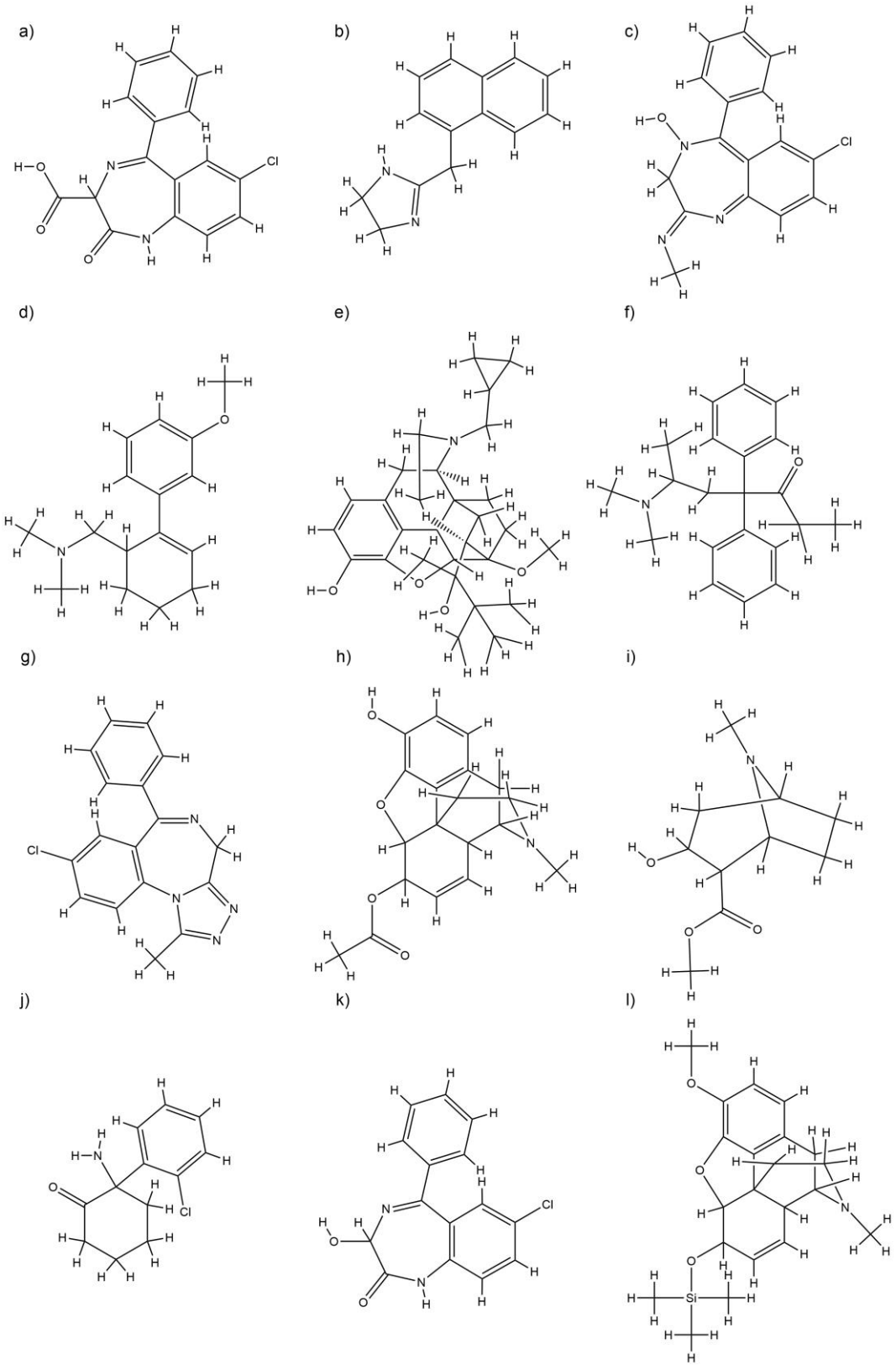

Scheme S1. Chemical structures of Clorazepate (a), Naphazoline (b), Chlordiazepoxide (c), Tramadol (d), Buprenorphine (e), Methadone (f), Alprazolam (g), 6-Monoacetylmorphine (h), Ecgonine methyl ester (i), Norketamine (j), Oxazepam (k) and Codeine (l).

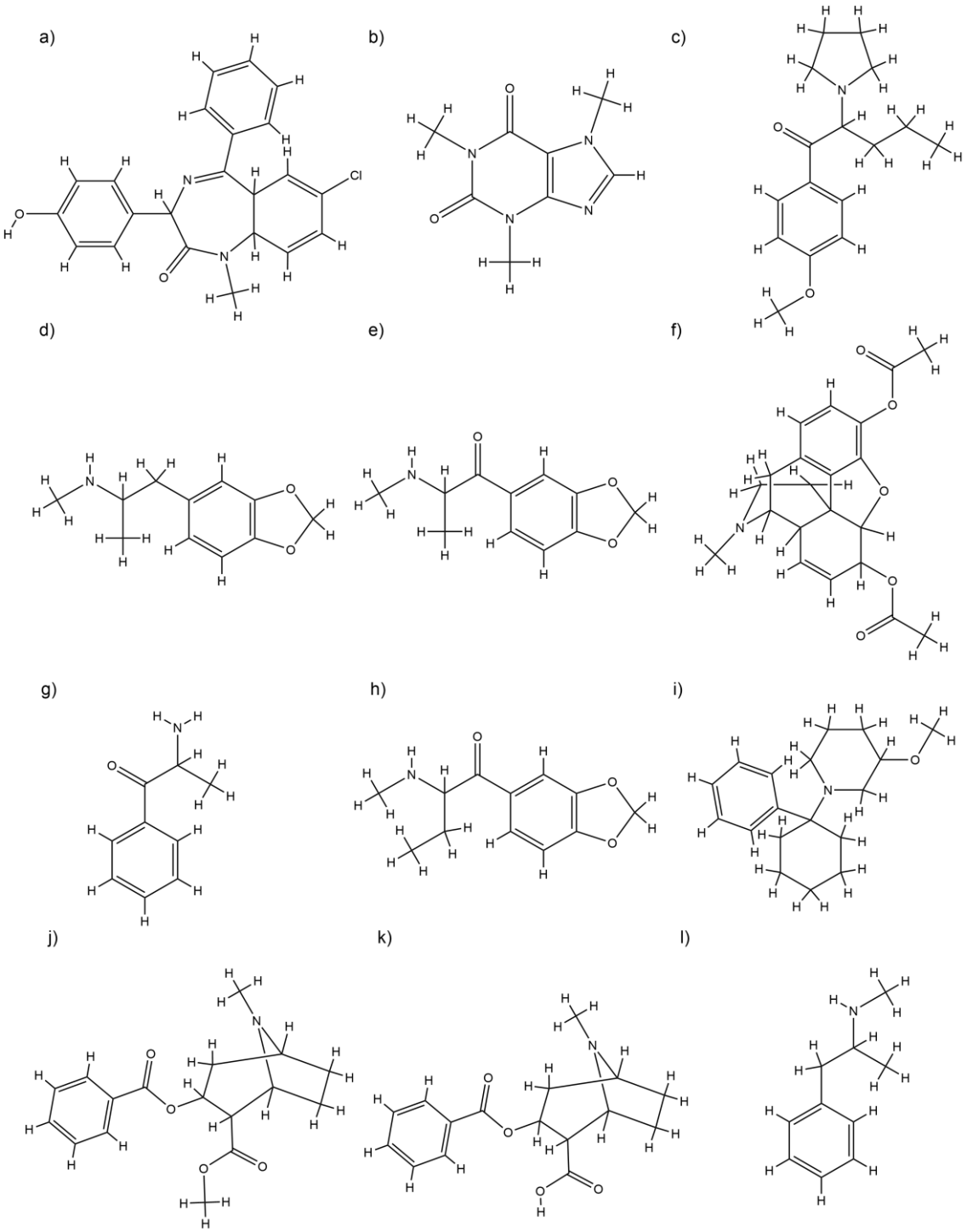

Scheme S2. Chemical structures of Diazepam (a), Caffeine (b), a-PVP (c), MDMA (d), Methylone (e), Heroine (f), Cathinone (g), Butylone (h), 3-Methoxyphencyclidine (i), Cocaine (j), Benzoylecgonine (k) and Metamphetamine (l).

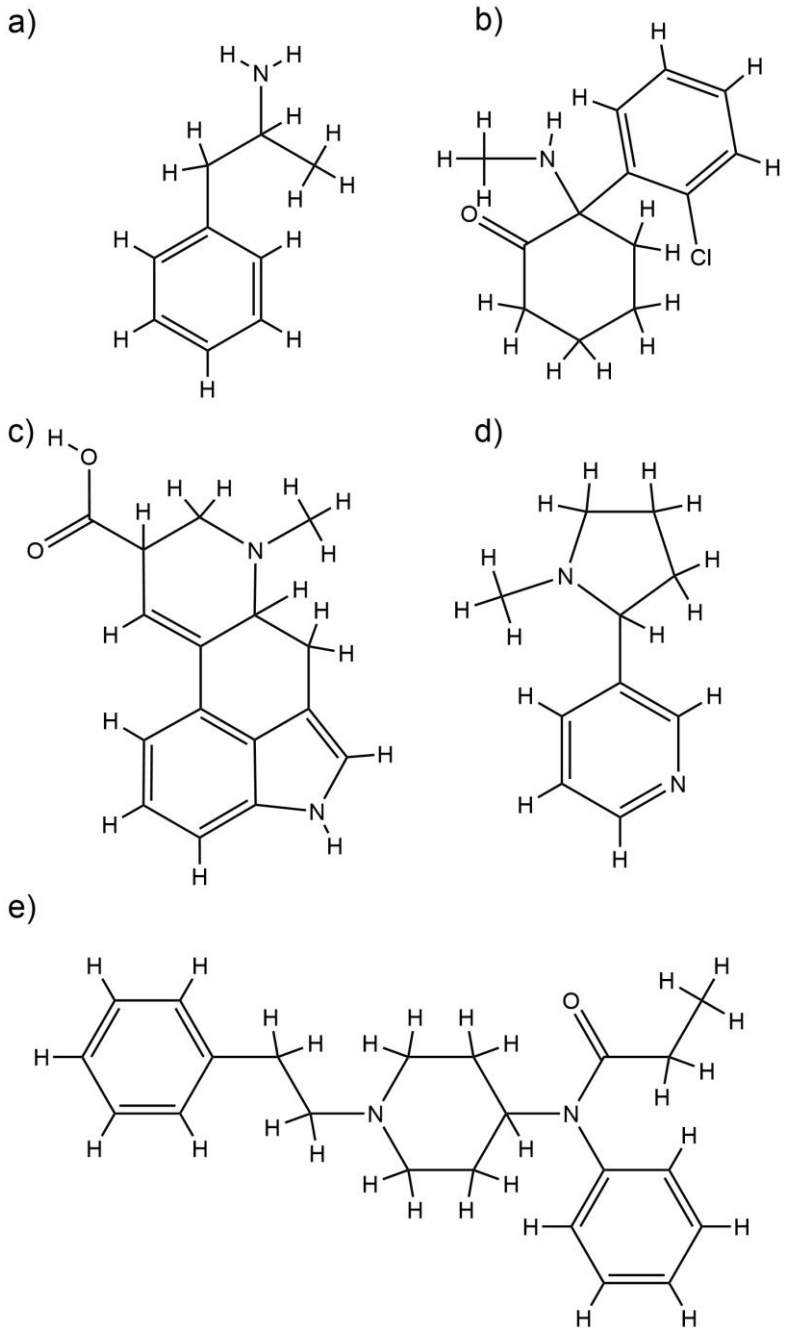

Scheme S3. Chemical structures of Amphetamine (a), Ketamine (b), LSD (c), Nicotine (d) and Fentanyl (e).

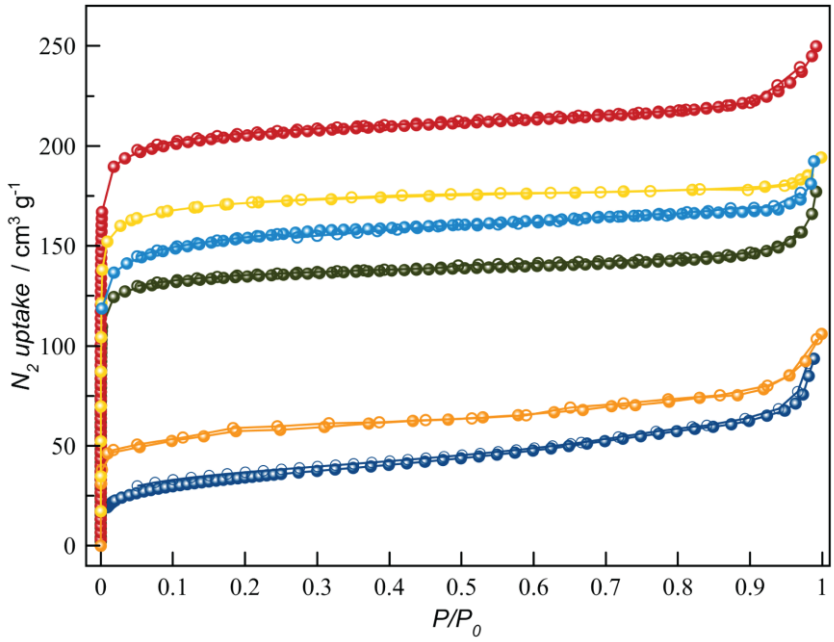

Figure S1. N_2 (77 K) adsorption isotherms for the activated compounds **1** (red), **2** (yellow), **3** (deep blue), **4** (light blue), **5** (green) and **6** (orange). Filled and empty symbols indicate the adsorption and desorption isotherms, respectively. The samples were activated at 70 °C under reduced pressure for 16 h prior to carry out the sorption measurements.

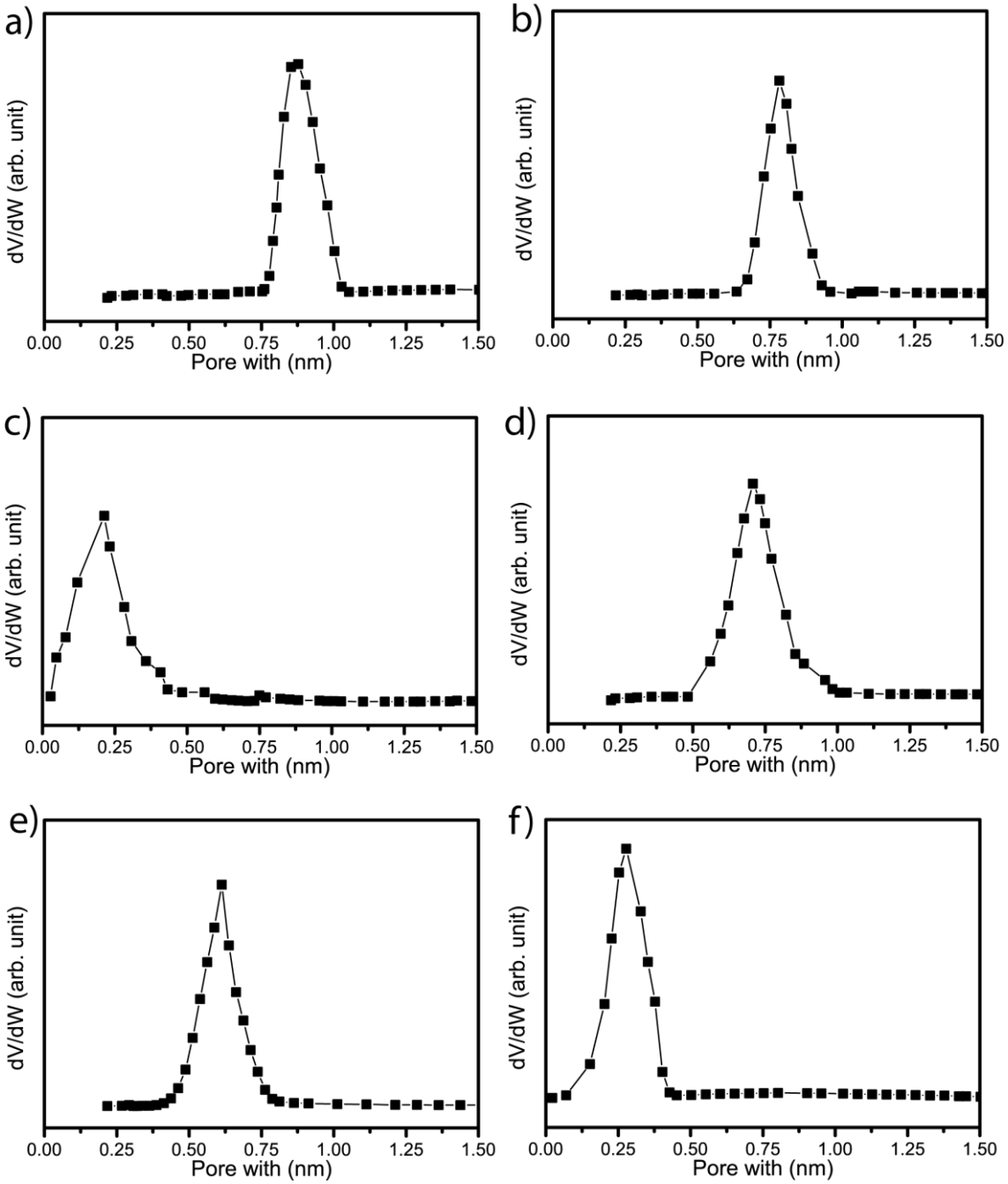

Figure S2. Pore size distribution plots for MOFs **1** (a), **2** (b), **3** (c), **4** (d), **5** (e) and **6** (f).

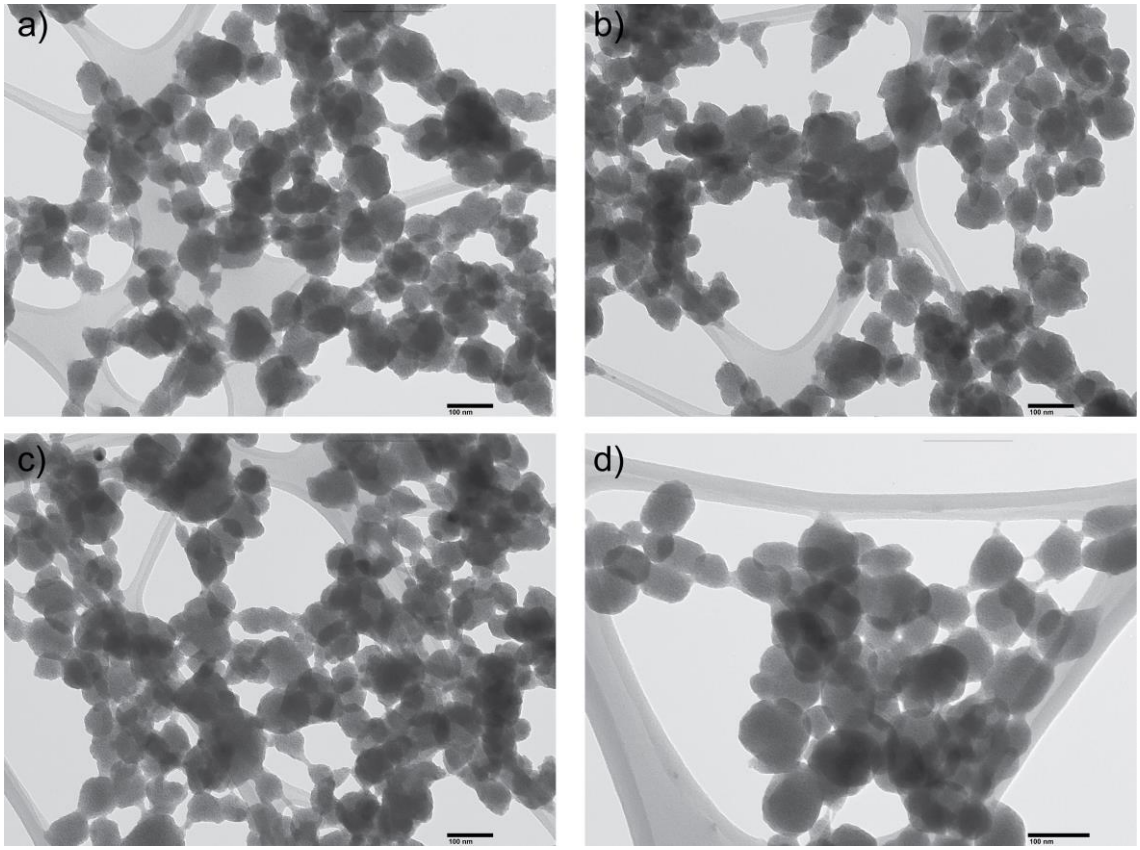

Figure S3. (a-d) TEM images of a polycrystalline sample of **3**.

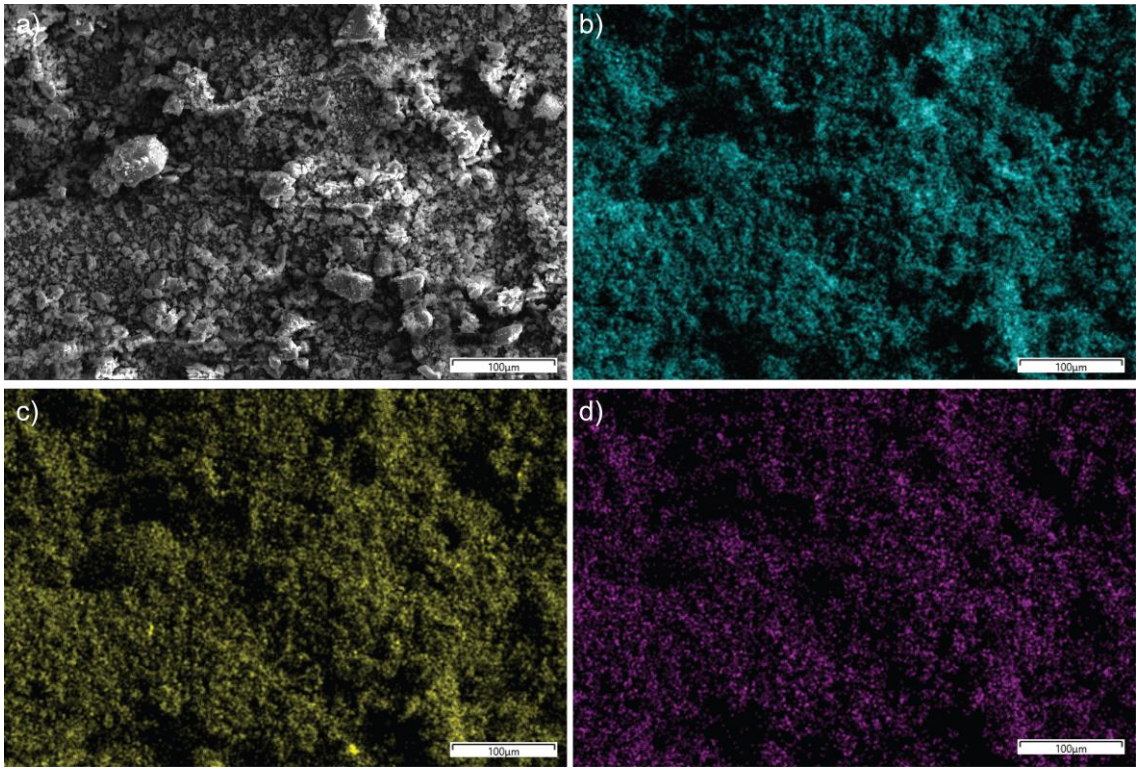

Figure S4. (a) SEM image of a polycrystalline sample of **3** and the corresponding EDX elemental mapping for Cu (b), Ca (c) and S (d) elements.

Figure S5. Image of the capture device incorporating SPE cartridges.

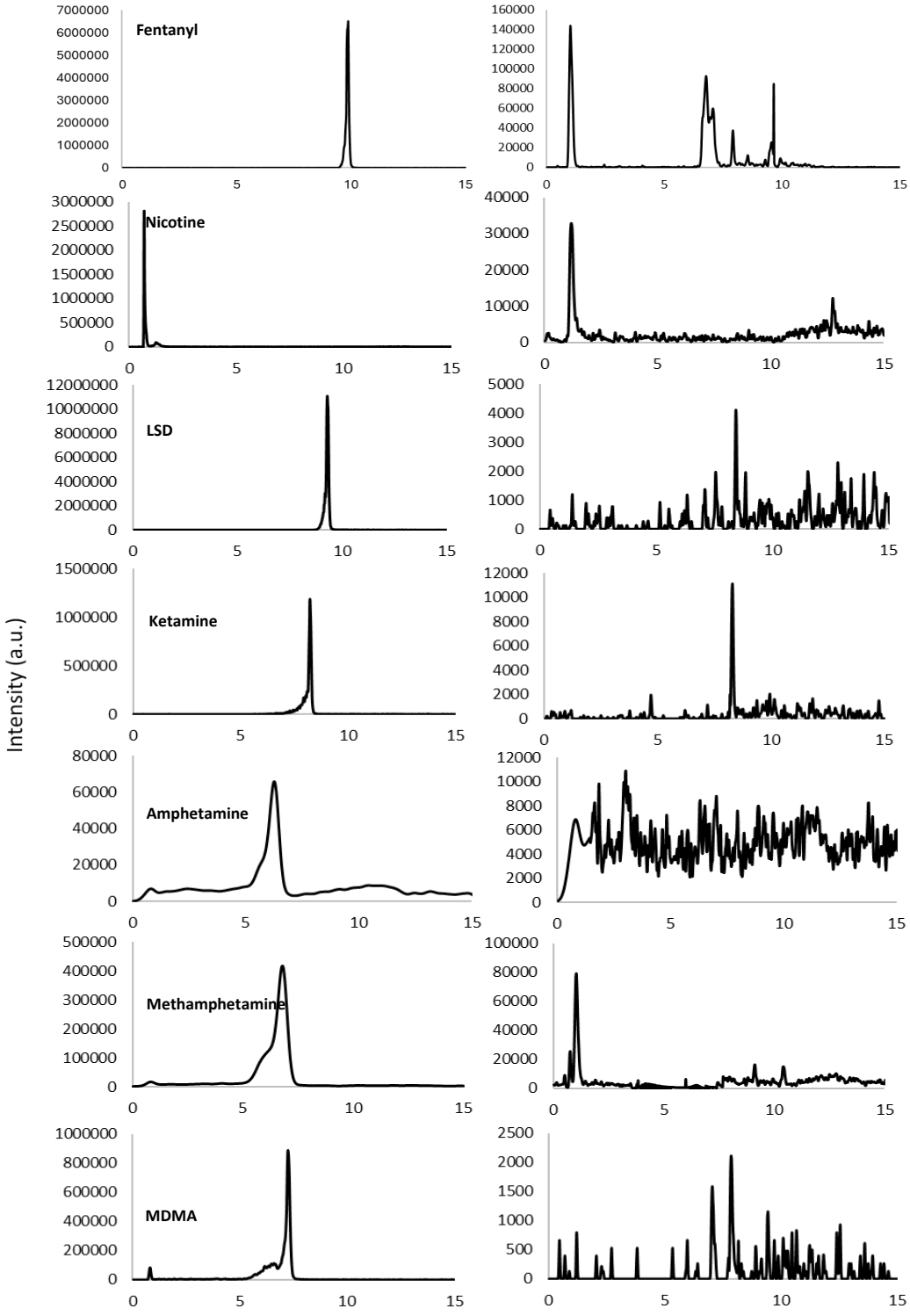
Fentanyl
Nicotine
LSD
Ketamine
Amphetamine
Methamphetamine
MDMA
Intensity (a.u.)
Time (min)

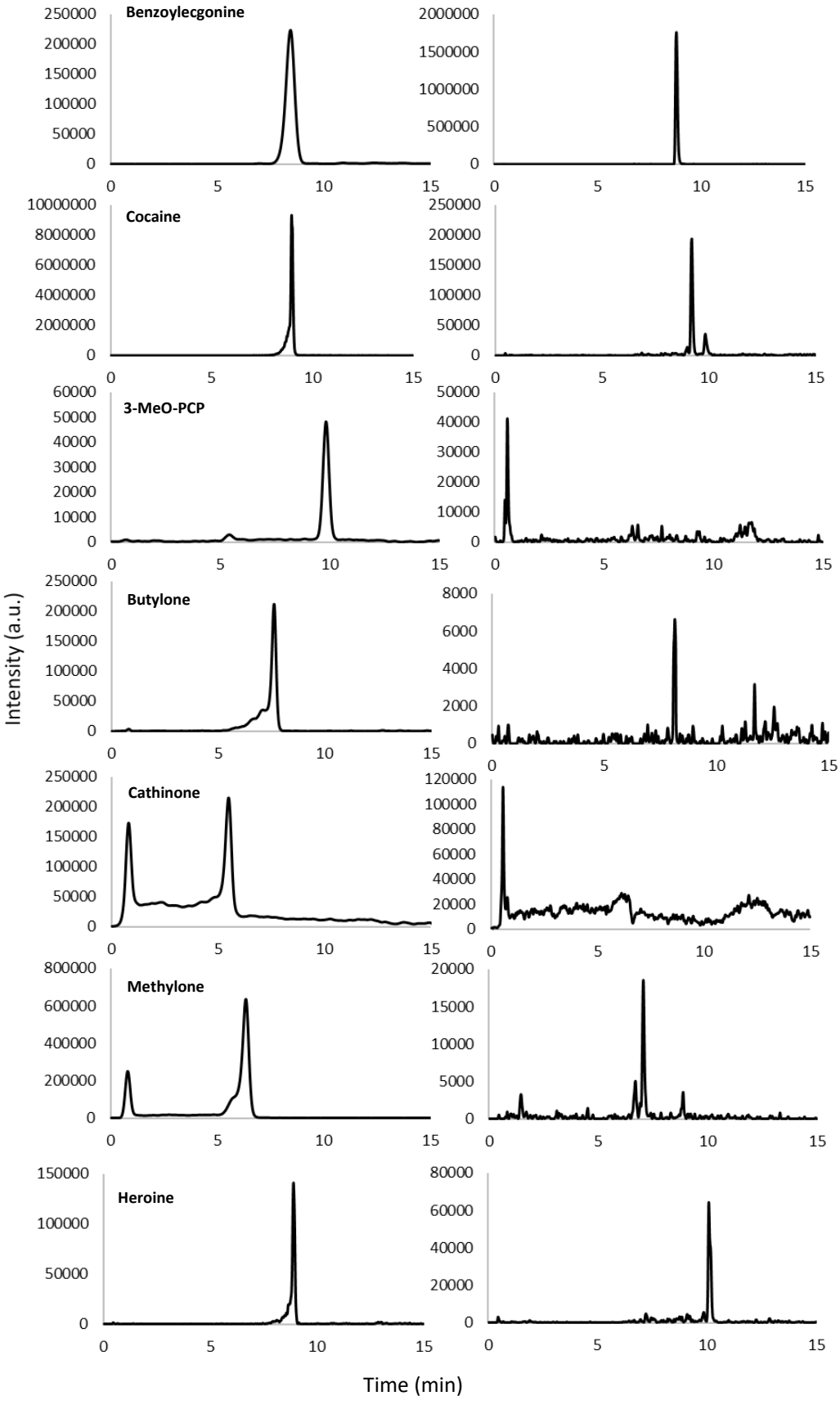
Benzoylecgonine
Cocaine
3-MeO-PCP
Butylone
Cathinone
Methylone
Heroine
Intensity (a.u.)
Time (min)

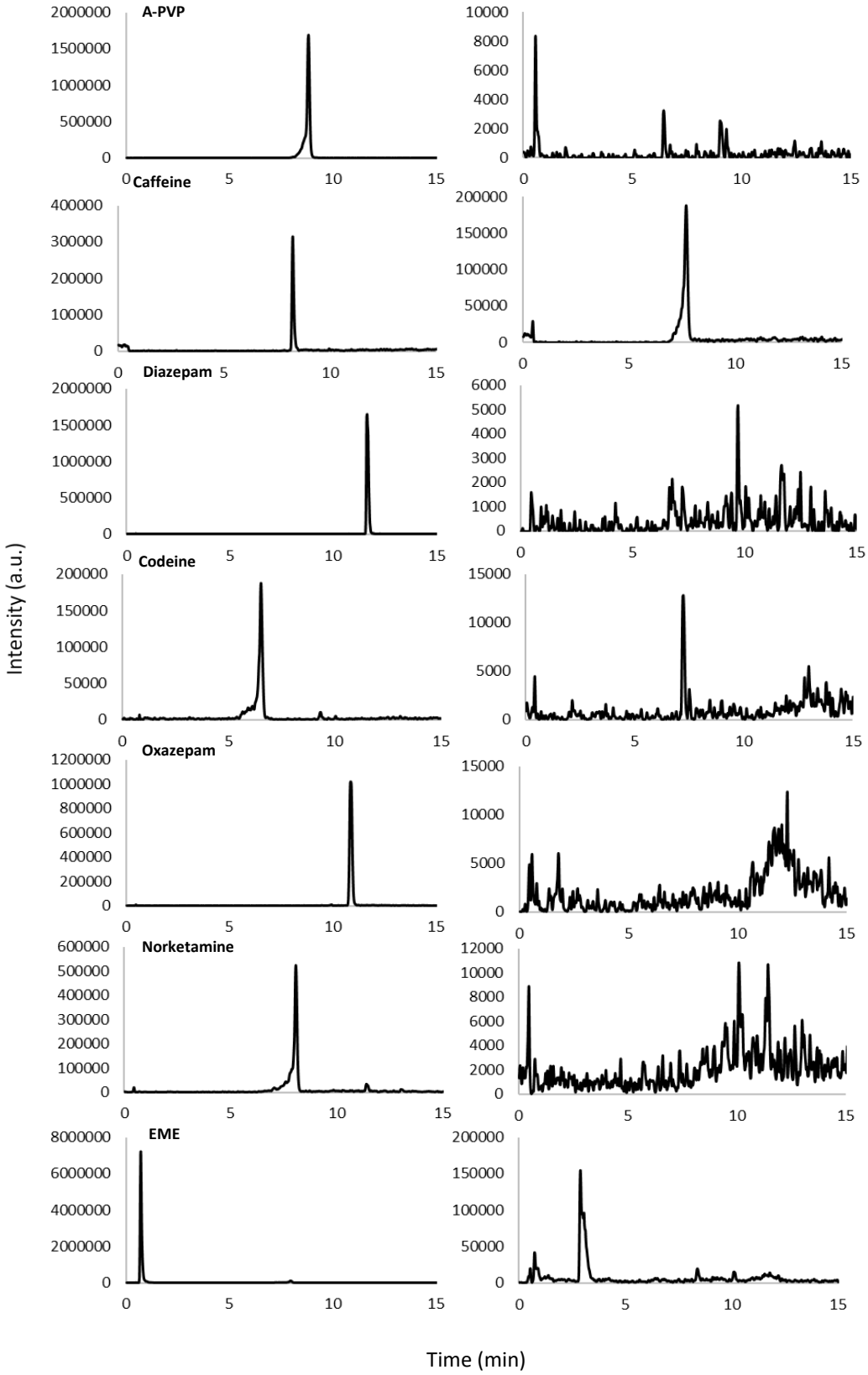
A-PVP
Caffeine
Diazepam
Codeine
Oxazepam
Norketamine
EME
Intensity (a.u.)
Time (min)

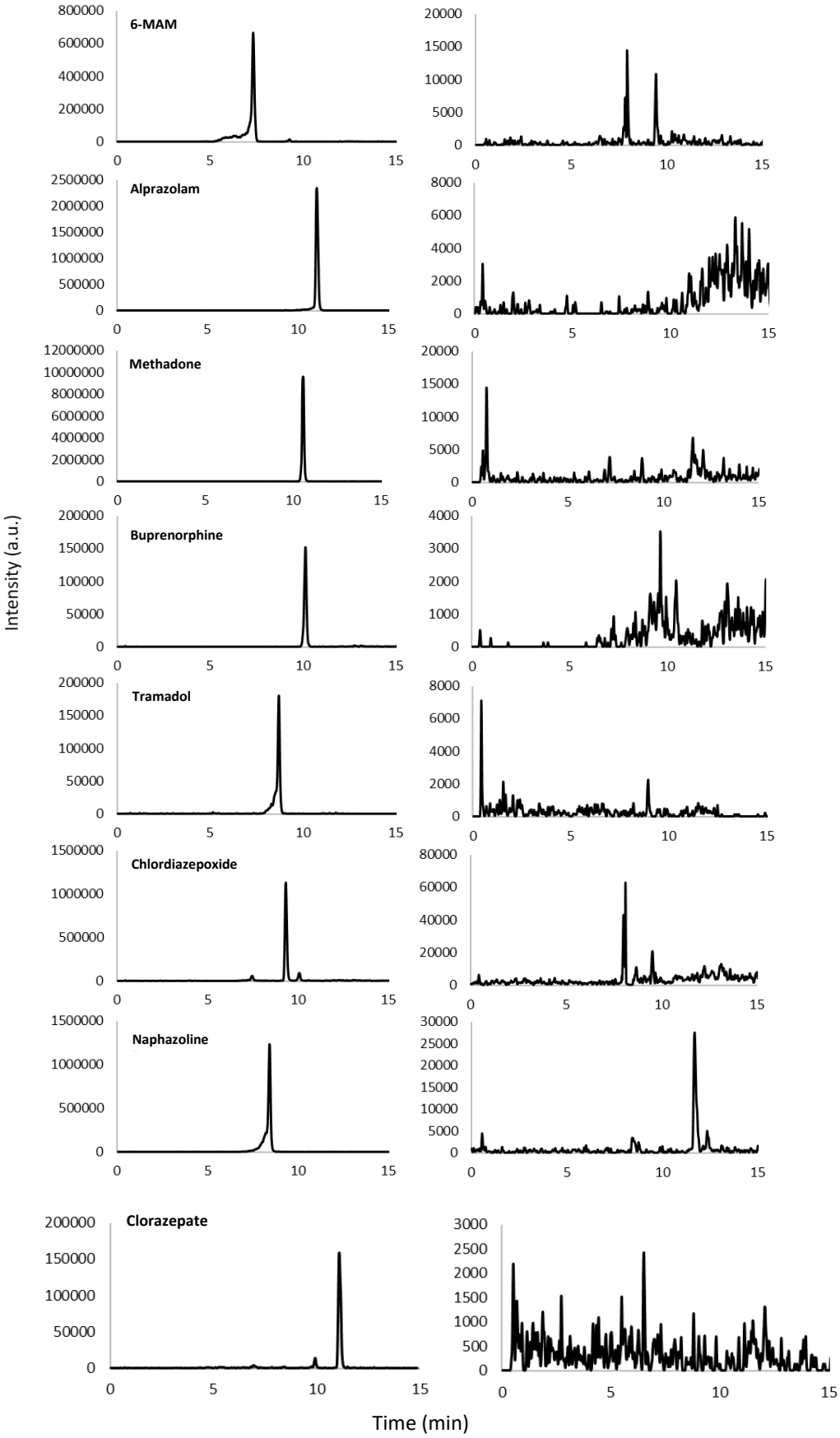

Figure S6. Extracted chromatograms for each analyte from (left) a 10 µg L^{-1} standard solution and (right) an extract obtained after loading a 10 µg L^{-1} aqueous solution through the MOF **3**.

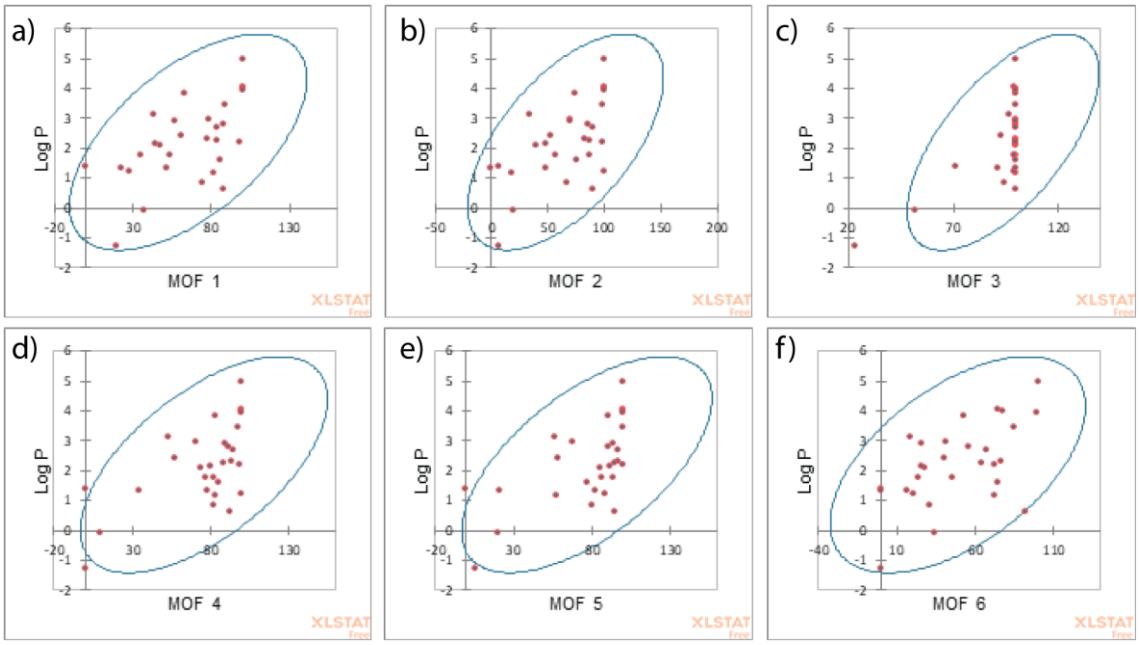

Figure S7. Octanol-water partition coefficient (LogP) of the 29 drugs studied in this work for MOFs **1** (a), **2** (b), **3** (c), **4** (d), **5** (e) and **6** (f).

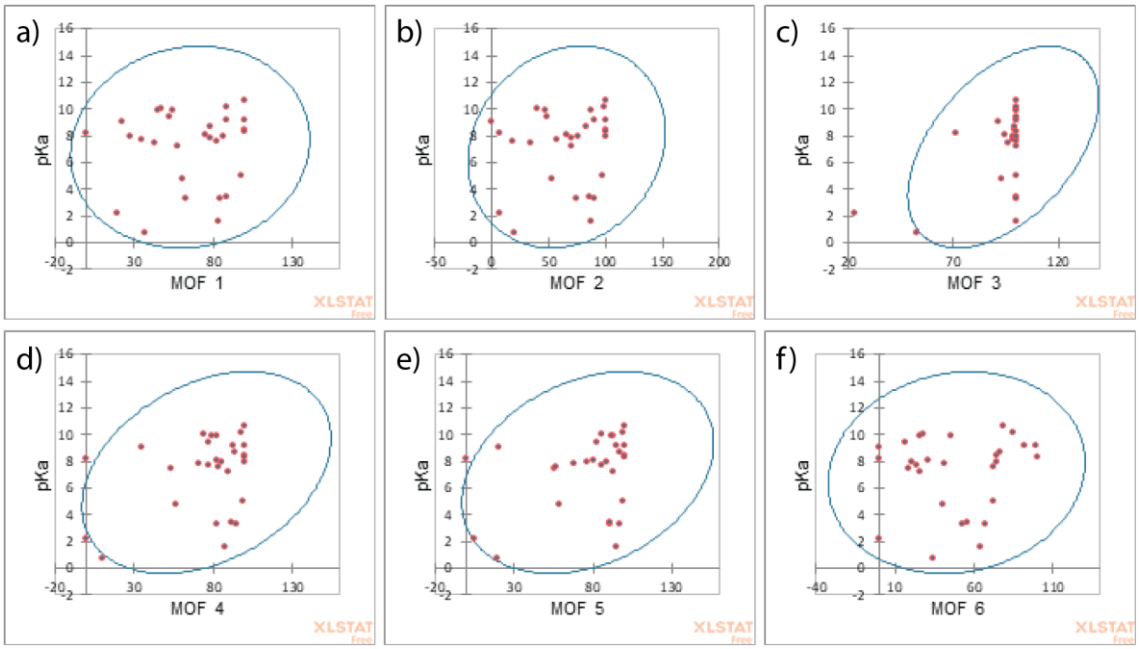

Figure S8. Acid dissociation constant (pKa) of the 29 drugs studied in this work for MOFs **1** (a), **2** (b), **3** (c), **4** (d), **5** (e) and **6** (f).

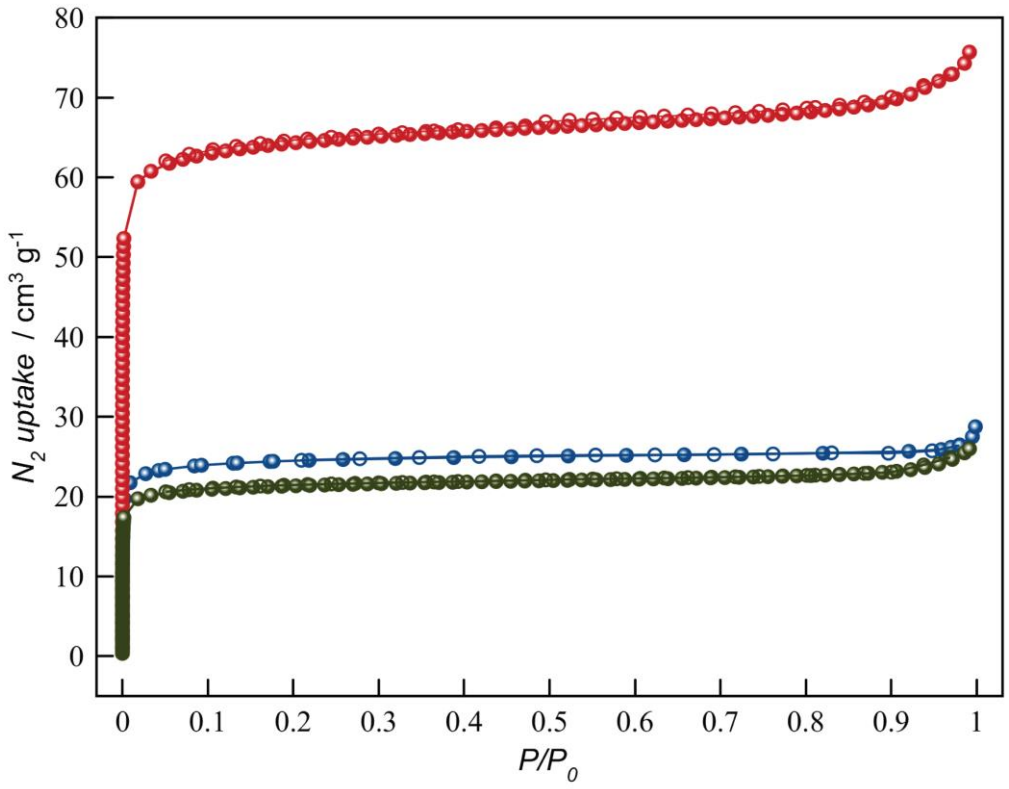

Figure S9. N_2 (77 K) adsorption isotherms for the activated compounds **amphetamine@2'** (red), **amphetamine@3** (green) and **fentanyl@3'** (blue). Filled and empty symbols indicate the adsorption and desorption isotherms, respectively. The sample was activated at 70 °C under reduced pressure for 16 h prior to carry out the sorption measurements.

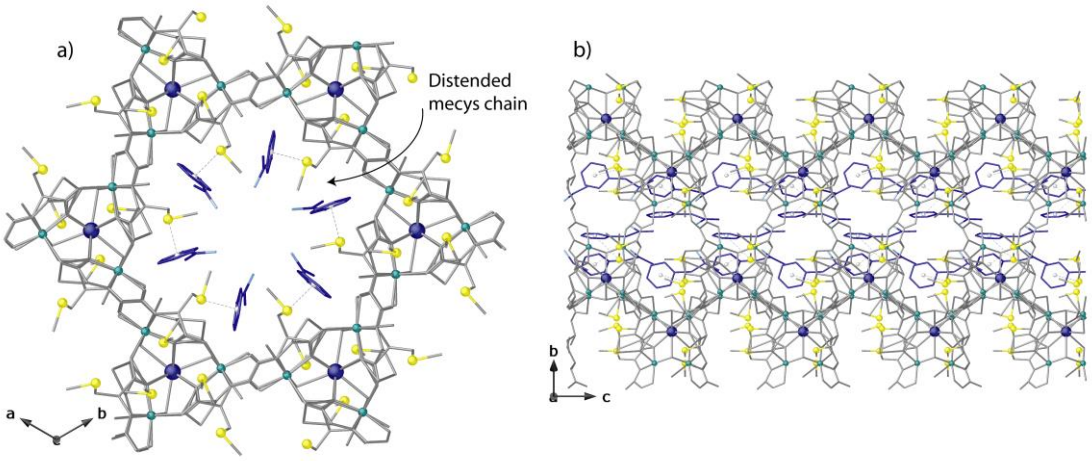

Figure S10. View of a single channel in the crystal structure of **amphetamine@2'** evidencing the most stable conformation of amphetamine guest molecules along *c* (a) and *a* crystallographic axis (b). Strontium and copper metal ions are represented by blue and cyan spheres, respectively; organic ligands, except for sulfur atoms (yellow spheres) and guest amphetamine molecules are represented with gray and blue sticks, respectively. Color code: grey: carbon atoms of the MOF network; light blue and deep blue: nitrogen atoms and carbon atoms of the amphetamine molecules, respectively.

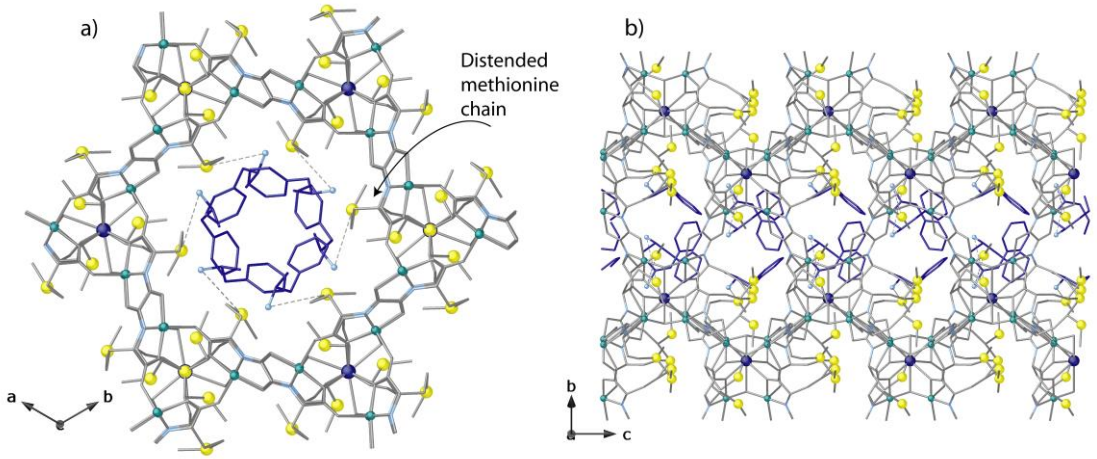

Figure S11. View of a single channel in the crystal structure of **amphetamine@3** evidencing the most stable conformation of amphetamine guest molecules along *c* (a) and *a* crystallographic axis (b). Calcium and copper metal ions are represented by blue and cyan spheres, respectively; organic ligands, except for sulfur atoms (yellow spheres) and guest amphetamine molecules are represented with gray and blue sticks, respectively. Color code: grey: carbon atoms of the MOF network; light blue and deep blue: nitrogen atoms and carbon atoms of the amphetamine molecules, respectively.

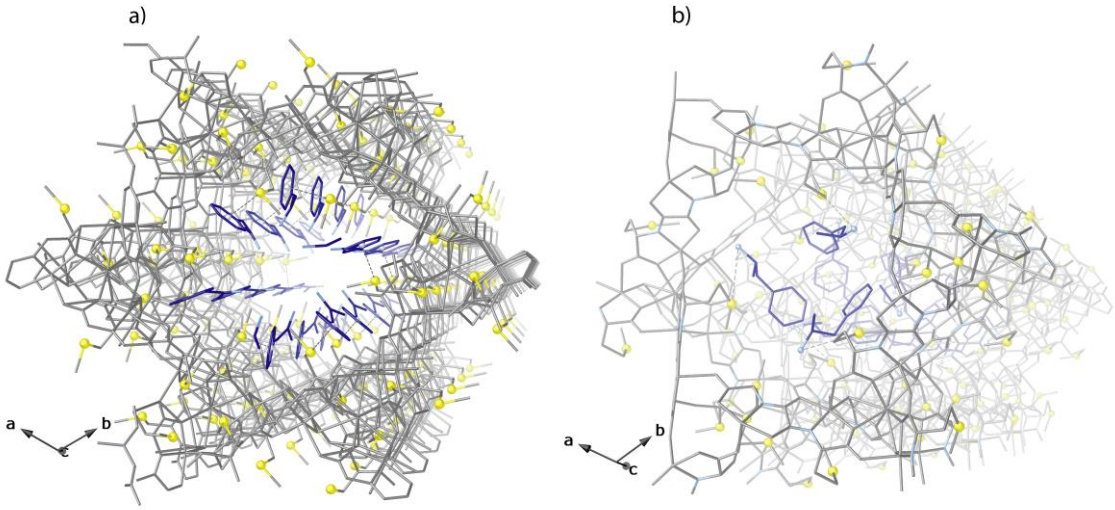

Figure S12. Perspective views in single channels generated in crystal structures of **amphetamine@2'** (a) and **amphetamine@3** (b) underlying the different orientations of targeted amphetamine molecules hosted in pores. Metal ions and organic ligands, except for sulfur atoms (yellow spheres) and guest amphetamine molecules are represented with grey and blue sticks, respectively. Color code: gray: carbon atoms of the MOF networks; light blue and deep blue: nitrogen atoms and carbon atoms of the amphetamine molecules, respectively.

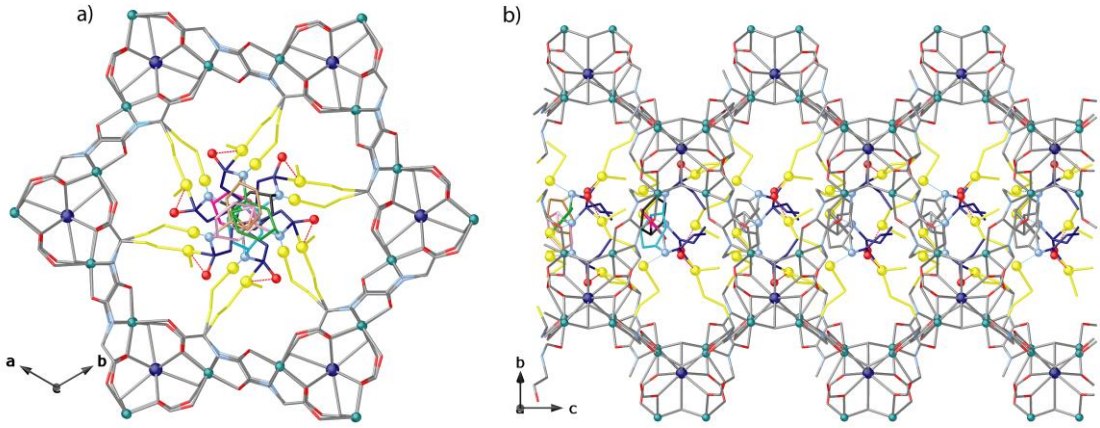

Figure S13. View of a single channel in the crystal structure of **fentanyl'@3'** showing the most stable conformations of fentanyl' guest molecules, depicted in different colors, along *c* (a) and *a* crystallographic axis (b). Strontium and copper metal ions are represented by blue and cyan spheres, respectively; organic ligands, except for sulfur atoms (yellow spheres) are represented with grey sticks, statistically disordered guest fentanyl' molecule cores are represented in purple, green or brown, respectively.

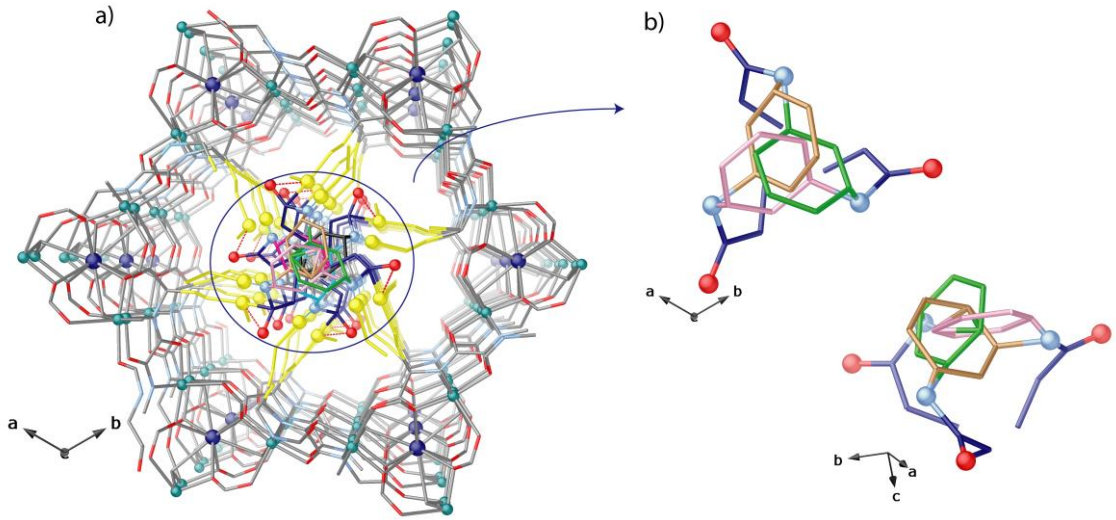

Figure S14. Perspective views in single channels generated in crystal structures of **fentanyl'@3'** (a) and two different views of **statistically disordered set of fentanyl' fragments** (b) underlying the different orientations of targeted fentanyl molecules hosted in pores. Strontium and copper metal ions are represented by blue and cyan spheres, respectively; organic ligands, except for sulfur atoms (yellow spheres) are represented with gray sticks, statistically disordered guest fentanyl' molecule cores are represented in purple, green or brown, respectively.

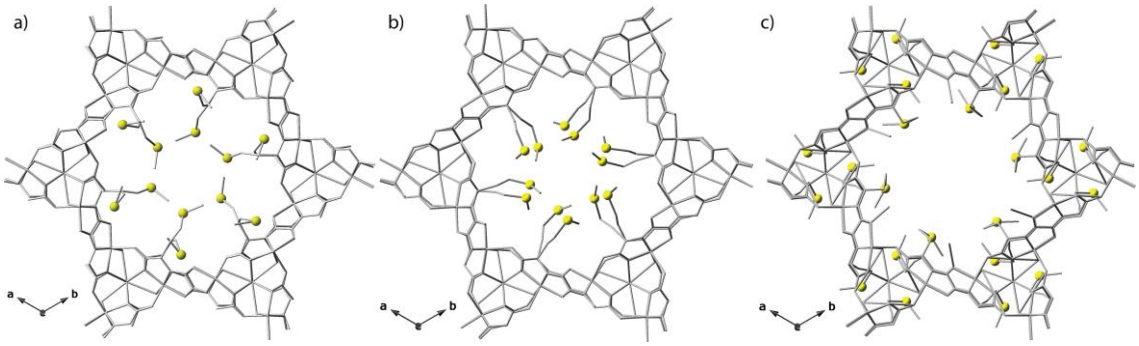

Figure S15. View of a single channel in the crystal structures of **3** (a), **amphetamine@3** (b) and **fentanyl'@3'** (c), along *c* crystallographic axis. Metal ions and organic ligands, except for sulfur atoms (yellow spheres), are represented with grey sticks. Guest molecules are omitted in order to visualise, more clearly, the conformation of thioether groups.

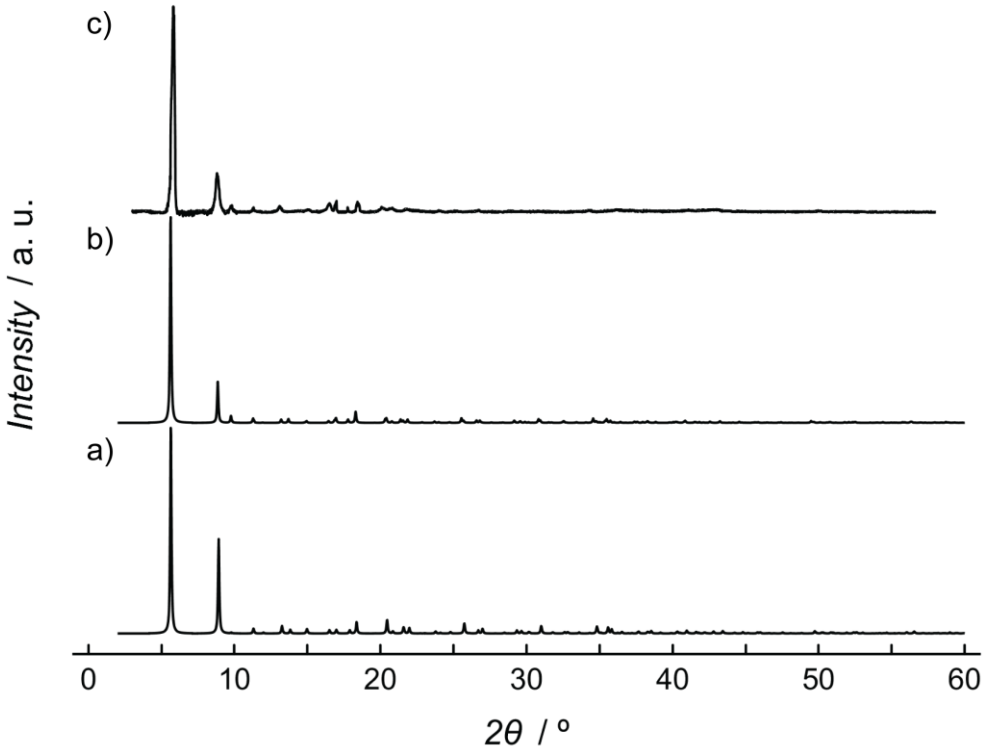

Figure S16. Theoretical PXRD patterns of MOF **2'** (a) and **amphetamine@2'** (b) and experimental PXRD patterns of **amphetamine@2'** (c) in the 2.0–60.0°.

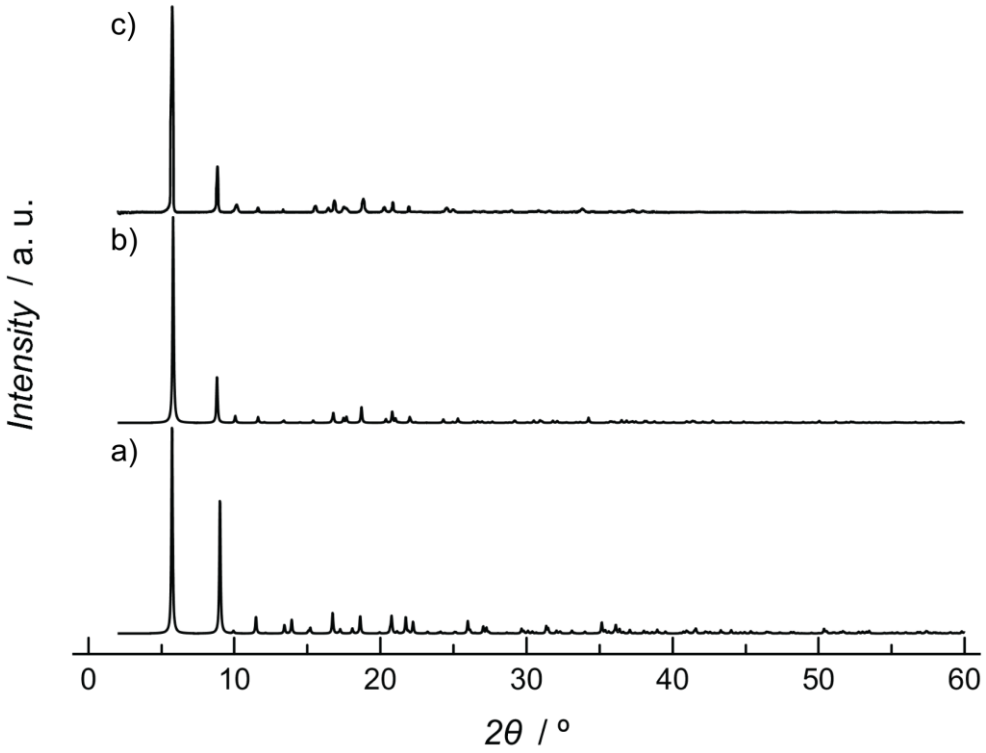

Figure S17. Theoretical PXRD patterns of MOF **3** (a) and **amphetamine@3** (b) and experimental PXRD patterns of **amphetamine @3** (c) in the 2.0–60.0°.

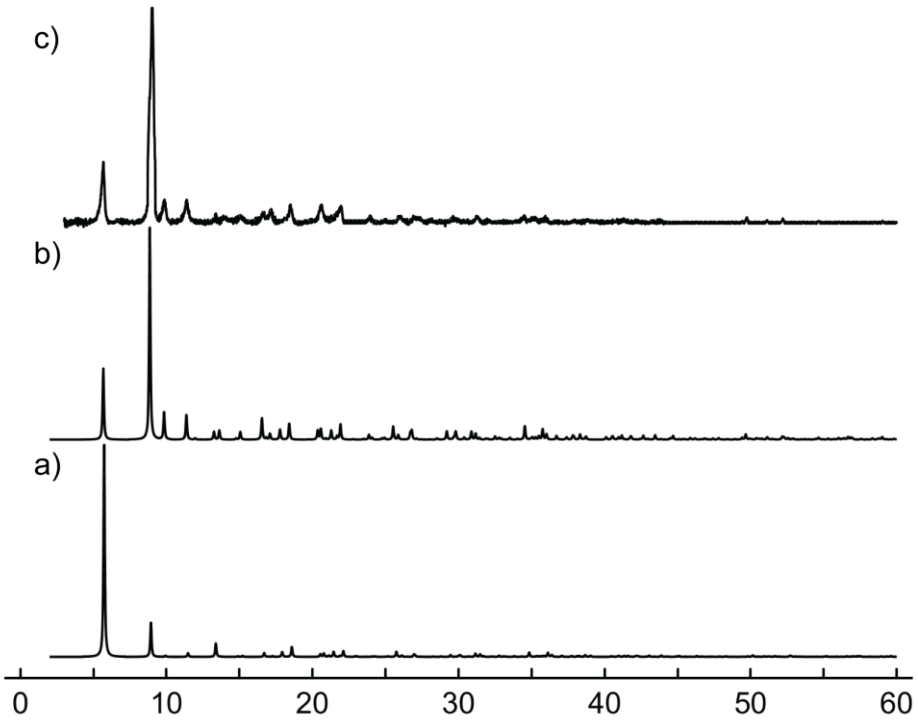

Figure S18. Theoretical PXRD patterns of MOF **3'** (a) and **fentanyl@3'** (b) and experimental PXRD patterns of **fentanyl@3'** (c) in the 2.0–60.0°.

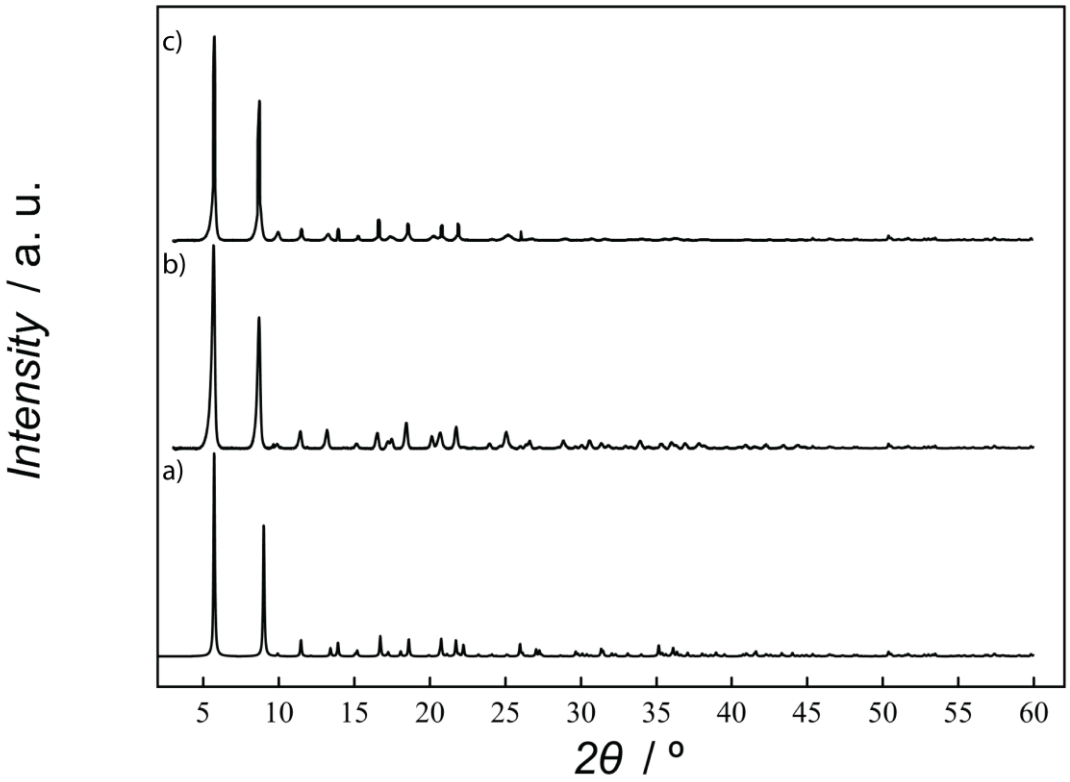

Figure S19. Theoretical (a) and experimental PXRD patterns of MOF **3** before (b) and after (c) the 16th reusability experiment in the 2.0–60.0°.

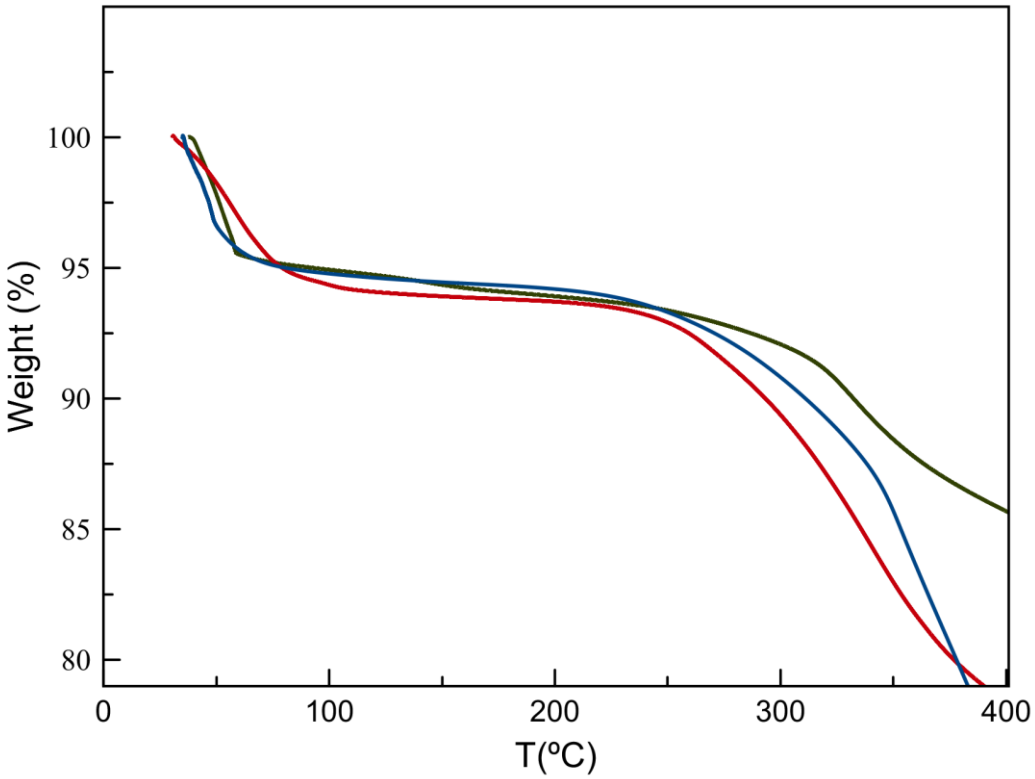

Figure S20. Thermo-Gravimetric Analysis (TGA) of **amphetamine@2'** (red), **amphetamine@3** (green) and **fentanyl@3'** (blue) under dry N_2 atmosphere.

References

1 M. Mon, R. Bruno, J. Ferrando-Soria, L. Bartella, L. Di Donna, M. Talia, R. Lappano, M. Maggiolini, D. Armentano and E. Pardo, *Mater. Horizons*, 2018, **5**, 683–690.

2 M. Mon, R. Bruno, E. Tiburcio, P.-E. Casteran, J. Ferrando-Soria, D. Armentano and E. Pardo, *Chem. Eur. J.*, 2018, **24**, 17712–17718.

3 R. Bruno, M. Mon, P. Escamilla, J. Ferrando-Soria, E. Esposito, A. Fuoco, M. Monteleone, J. C. Jansen, R. Elliani, A. Tagarelli, D. Armentano and E. Pardo, *Adv. Funct. Mater.*, 2021, **31**, 2008499.

4 E. Tiburcio, R. Greco, M. Mon, J. Ballesteros-Soberanas, J. Ferrando-Soria, M. López-Haro, J. C. Hernández-Garrido, J. Oliver-Meseguer, C. Marini, M. Boronat, D. Armentano, A. Leyva-Pérez and E. Pardo, *J. Am. Chem. Soc.*, 2021, **143**, 2581–2592.

5 M. Mon, F. Lloret, J. Ferrando-Soria, C. Martí-Gastaldo, D. Armentano and E. Pardo, *Angew. Chemie Int. Ed.*, 2016, **55**, 11167–11172.

6 M. Mon, J. Ferrando-Soria, T. Grancha, F. R. Fortea-Pérez, J. Gascon, A. Leyva-Pérez, D. Armentano and E. Pardo, *J. Am. Chem. Soc.*, 2016, **138**, 7864–7867.

7 M. Mon, R. Bruno, E. Tiburcio, M. Viciano-Chumillas, L. H. G. Kalinke, J. Ferrando-Soria, D. Armentano and E. Pardo, *J. Am. Chem. Soc.*, 2019, **141**, 13601–13609.

8 M. Baratta, T. F. Mastropietro, R. Bruno, A. Tursi, C. Negro, J. Ferrando-Soria, A. I. Mashin, A. Nezhdanov, F. P. Nicoletta, G. De Filpo, E. Pardo and D. Armentano, *ACS Appl. Nano Mater.*, 2022, **5**, 5223–5233.

9 C. Negro, H. Martínez Pérez-Cejuela, E. F. Simó-Alfonso, J. M. Herrero-Martínez, R. Bruno, D. Armentano, J. Ferrando-Soria and E. Pardo, *ACS Appl. Mater. Interfaces*, 2021, **13**, 28424–28432.

10 J. Navarro-Alapont, C. Negro, S. Navalón, A. Dhakshinamoorthy, D. Armentano, J. Ferrando-Soria and E. Pardo, *Inorg. Chem.*, 2024, **63**, 13681–13688.

11 C. Negro, P. Escamilla, R. Bruno, J. Ferrando-Soria, D. Armentano and E. Pardo, *Chem. – A Eur. J.*, 2022, **28**, e202200034.

12 C. Negro, H. Martínez Pérez-Cejuela, E. F. Simó-Alfonso, W. Iqbal, J. M. Herrero-Martínez, D. Armentano, J. Ferrando-Soria and E. Pardo, *ACS Appl. Mater. Interfaces*, 2023, **15**, 3069–3076.

13 W. SAINT, version 6.45, Bruker Analytical X-ray Systems, Madison, 2003.

14 W. Sheldrick G.M. SADABS Program for Absorption Correction, version 2.10, Analytical X-ray Systems, Madison, 2003.

15 G. M. Sheldrick, *Acta Crystallogr. A.*, 2008, **64**, 112–22.

16 G. M. Sheldrick, *Acta Crystallogr. Sect. C Struct. Chem.*, 2015, **71**, 3–8.

17 W. S.-2013/4 B. A. X. I. Madison, 2013.

18 A. L. Spek, *Acta Crystallogr. Sect. C Struct. Chem.*, 2015, **71**, 9–18.

19 A. L. Spek, *Acta Crystallogr. Sect. D Biol. Crystallogr.*, 2009, **65**, 148–155.

20 L. J. Farrugia, *J. Appl. Crystallogr.*, 1999, **32**, 837–838.

21 C. Palmer, D. CRYSTAL MAKER, Cambridge University Technical Services, 1996.